On the Development of Coherent Structure in a Plane Jet*
(Part 3, Multi-Point Simultaneous Measurement of Main Streamwise Velocity and the Reconstruction of Velocity Field by the KL Expansion)

Yasuhiko SAKAI**, Nobuhiko TANAKA***,
Mutsumi YAMAMOTO**** and Takehiro KUSHIDA**

In order to clarify the dynamics of the coherent structure in a turbulent plane jet, the simultaneous measurement of the main streamwise velocity at 21 points in the self-preserving region of a turbulent plane jet has been performed by an array of I-type hot-wire probes. Then the KL (Karhunen-Loève) expansion was applied to extract the coherent structure in the jet. The total number of eigenfunctions (modes) is $N = 21$, which corresponds to the number of probes. The eigenfunctions (modes) are numbered in order of magnitude of their corresponding eigenvalues. From the investigation of the random coefficients and the eigenfunctions (modes), it is found that the low-numbered (energetic) modes represent the large scale (coherent) structure, the middle-numbered modes represent the finer (small-scale) random structure, and the higher-numbered modes contribute mainly to the intermittent structure in the outer edge region. From the spatio-temporal velocity field reconstructed by the first KL mode, it is found that there exist a pair of fluid lumps with the positive and negative streamwise velocity fluctuation on the opposite sides of the jet centerline, and the signs of velocity fluctuation for those fluid lumps change alternately as time proceeds. These characteristics are consistent with the so called "jet flapping" phenomenon.

Key Words: Jet, Turbulence, Vortex, Flow Measurements, Spatial Velocity Correlation, Karhunen Loève Expansion, Coherent Structure, Flapping Phenomenon

1. Introduction

Although the coherent structure observed in turbulent flow is generally recognized as the deterministic fluid motion, its occurrence is irregular in both space and time. So the "conditional" technique[1] has been commonly used to extract the phenomenon characterizing the coherent structure and examine the mean feature for a period of time that its structure appears. In the usual conditional techniques, a physical quantity at a reference position was measured and some criterion (condition) on this quantity was imposed to extract various statistics. However, this criterion was often determined from a subjective point of view to extract the expecting structure. In this study, to extract the coherent structure "non-conditionally (objectively)" from the turbulent field, the Karhunen-Loève (KL) expansion[2]-[5] was applied. The KL expansion is also referred to as the Proper Orthogonal Decomposition (POD), which is a mathematical technique based on the two-point velocity correlation tensor to capture the energetic structure in the inhomogeneous turbulence. The object of present study is a turbulent plane jet which is of simple geometry and important in a very wide variety of engineering applications. In our previous works[6],[7], we performed the simultaneous measurements at two points with the X-type hot wire probes in the three downstream regions of a turbulent plane jet (the potential core region, the interaction region and the self-preserving region) and investigated the development of the coherent structure in a viewpoint of two-point spatial correlations, eigenvalues and eigenfunctions of the KL expansion. In this time, the simultaneous measurement of the main streamwise velocity at 21 points in the self-

* Received 5th June, 2006 (No. 04-1049). Japanese Original: Trans. Jpn. Soc. Mech. Eng., Vol.71, No.708, B (2005), pp.1986–1993 (Received 21st September, 2004)

** Department of Mechanical Science and Engineering, Nagoya University, Furo-cho, Chikusa-ku, Nagoya 464–8603, Japan. E-mail: ysakai@mech.nagoya-u.ac.jp

*** Mitsubishi Heavy Industries, Ltd., 1–1 Akunoura-machi, Nagasaki 850–8610, Japan

**** Toyota Industries Corporation, 2–1 Toyoda-cho, Kariya 448–8671, Japan

preserving region of the plane jet has been performed by an array of I-type hot wire probes, then the unsteady spatial structure of the velocity field are examined. In particular, by the reconstruction of velocity filed with the KL expansion, the details of spatio-temporal coherent structure called "flapping" phenomenon are investigated. In this report, these results are presented.

2. Experimental Methods and Conditions

Figure 1 shows the schematic of experimental apparatus near the two-dimensional nozzle exit and the coordinate system. The skimmer was installed at the position of about 1 mm downstream from the nozzle exit to eliminate the boundary layer which develops along the contraction wall. The height d and the width l of the skimmer exit are 12 mm and 236 mm, respectively. With this skimmer, only the uniform part of the nozzle exit flow can be extracted and the initial mean streamwise velocity profile of the jet is almost of a "top-hat" shape[8]. Further, the sidewall was set vertically at the test section to inhibit the entrainment from the surrounding. With the use of the sidewall, a good 2-dimensional flow field at the test section could be realized[8]. In this study, the velocity of the skimmer exit U_0 is about 20 m/s, so Reynolds number $Re(=U_0 d/\nu)$ is about 16 000. The coordinate system is as follows: the axial (streamwise) coordinate is x_1, the vertical (cross-streamwise) coordinate is x_2 and the spanwise coordinate is x_3. In the simultaneous measurement, the 21 I-type hot-wire neighboring probes are spaced in the inhomogeneous x_2-direction with $\Delta r = 7.5$ mm (which is the interval between probes). Figure 2 shows the arrangement of the rake of I-type hot-wire probes. The measurements are performed at seven downstream locations, i.e., x_1/d = 10.0, 15.0, 20.0, 25.0, 30.0, 35.0, 40.0. Here it is noted that since the interval Δr between probes is constant, the information of the outer edge can not be captured accurately in the far downstream region because of the spread of the jet. Therefore in this study we mainly deal with the data at x_1/d = 20.0, which cover almost whole velocity field of the jet ($-2.5 < x_2/b < 2.5$). The schematic of the multi-point measurement system is also shown in Fig. 2. In this system, 3 hot-wire anemometries on the market (KANOMAX MODEL 1011 (2ch) and HAYAKAWA MODEL HC30 (1ch)) were used, but other 18 hot-wire anemometries (18ch) are handmade in our laboratory. These handmade anemometries give a frequency response −3 dB down at approximately 14 kHz. In this study, the sampling frequency is 10 kHz and the number of sampling data is 229 376. The calibrations of hot-wire anemometries were made by using the potential core of the jet (See Ref. (8) for the details of the calibration method).

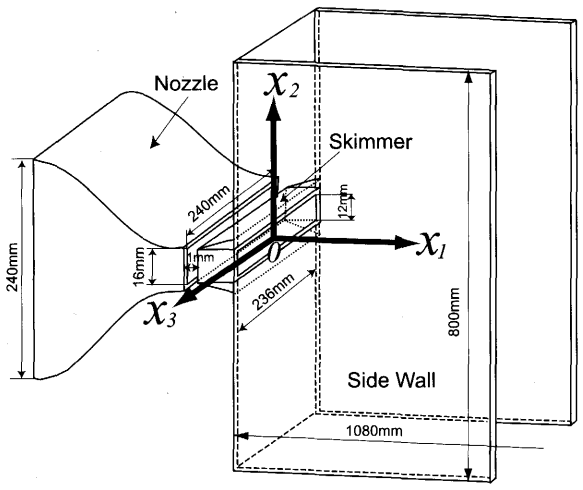

Fig. 1 Schematic of the experimental apparatus near the nozzle exit and the coordinate system

3. Karhunen-Loève Expansion

Here, we summarize the theory of the KL expansion (see Refs. (2)–(6) for details). Eigenfunctions $\phi_u^{(n)}(x)$ and eigenvalues $\lambda_u^{(n)}$ of the KL expansion for one component u of the velocity vector $\boldsymbol{u}$ are given as the solution of the following eigenvalues problem of the two-point spatial velocity correlation $R_{uu}(x_2, x_2')$[(2)–(4)],

$$\sum_{j=1}^{N} R_{uu}(x_2^{(i)}, x_2^{(j)}) w(x_2^{(j)}) \phi_u^{(n)}(x^{(j)}) \Delta r = \lambda_u^{(n)} \phi_u^{(n)}(x_2^{(i)}), \quad (1)$$

$$R_{uu}(x_2, x_2') = \langle u(x_2, t) u(x_2', t) \rangle, \quad (2)$$

where x_2 and x_2' denote the cross-streamwise coordinate (see Fig. 1), then $x_2^{(i)}$ and $x_2^{(j)}$ correspond to the measurement position of each probe. N is the number of I-type hot-wire probes and $\langle \cdot \rangle$ denotes an ensemble average. $w(x_2^{(j)})$ is j-component of the following N-dimensional weighting vector $\boldsymbol{w}$,

$$w(x^{(j)}) = [0.5, \overbrace{1, 1, \cdots, 1}^{N-2}, 0.5]. \quad (3)$$

The important properties of the KL expansion are summarized as follows.

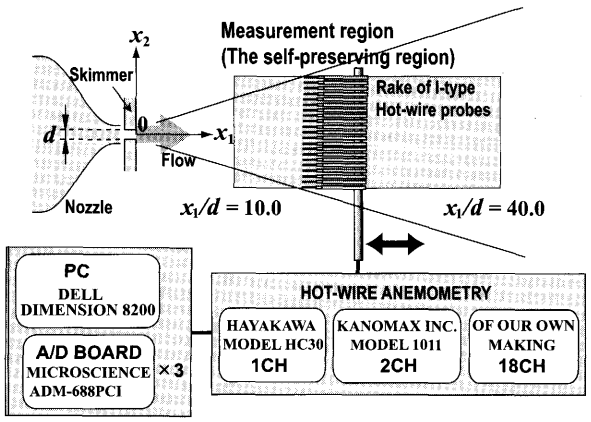

Fig. 2 Multi-point measurement system

(a) The eigenvalues are real, and those are usually arranged in order of magnitude

$$\lambda_u^{(1)} > \lambda_u^{(2)} > \lambda_u^{(3)} \cdots. \tag{4}$$

(b) The velocity field can be expressed as a linear combination of the eigenfunctions

$$u(x_2,t) = \sum_{n=1}^{\infty} a_u^{(n)}(t)\phi_u^{(n)}(x_2), \tag{5}$$

where from the orthogonality of the eigenfunctions the random coefficients $a_u^{(n)}(t)$ is obtained as follows

$$a_u^{(n)}(t) = \int_I u(x_2,t)\phi_u^{(n)}(x_2)\mathrm{d}x_2. \tag{6}$$

I is a domain for the KL expansion to be applied.

(c) The integral of the mean square value of the fluctuating velocity u in the domain I is given by the sum of the eigenvalues,

$$E_u = \int_I \left\langle u^2(x_2,t)\right\rangle \mathrm{d}x_2 = \sum_{n=1}^{N} \lambda_u^{(n)}, \tag{7}$$

$$\left\langle u^2(x_2,t)\right\rangle = \sum_{n=1}^{N} \lambda_u^{(n)} \left\{\phi_u^{(n)}(x_2)\right\}^2. \tag{8}$$

4. Experimental Results

4.1 Profiles of mean velocity and r.m.s. velocity

Figures 3 and 4 present the vertical profiles of the streamwise mean velocity U and the streamwise r.m.s. velocity u' at $x_1/d = 20.0$ and 30.0, respectively. The ordinate and the abscissa of both profiles are normalized by the mean streamwise velocity of the jet centerline U_m and the half width b, respectively. Both profiles are obtained by "one sampling" data of about 23 sec at the simultaneous measurement with an array of 21 I-type hot-wire probes. The solid lines in Figs. 3 and 4 are the profiles obtained by velocity measurements with a single X-type hot-wire probe at $x_1/d = 20.0$[6]. It is found that the data of the 21-point measurement agrees very well with those of the measurement with the single X-type probe. Therefore we concluded that the present simultaneous measurements at 21 points with the I-type hot-wire probes are sufficiently reliable.

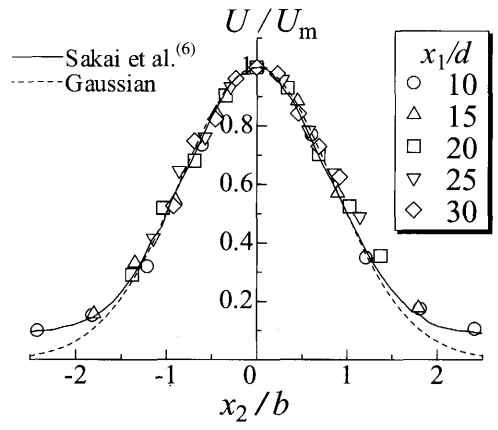

Fig. 3 Vertical profiles of the streamwise mean velocity U

4.2 Two-point spatial velocity correlation

Figure 5 shows the two-point spatial velocity correlation coefficient for u at $x_1/d = 20.0$. The two-point spatial velocity correlation coefficient[9] is defined by

$$C_{uu}(x_2,x_2') = \frac{\left\langle u(x_2,t)u(x_2',t)\right\rangle}{\sqrt{\left\langle u^2(x_2,t)\right\rangle}\sqrt{\left\langle u^2(x_2',t)\right\rangle}}, \tag{9}$$

The present profile in Fig. 5 agrees very well with the two-point spatial velocity correlation coefficient of the simultaneous measurements at two points with the X-type hot-wire probes reported by Sakai et al.[6] Since C_{uu} is the dimensionless quantity of R_{uu} in the KL expansion (see Eq. (1)), this agreement warrants the reliability of the results of the KL expansion. From Fig. 5, it is found that C_{uu} is negative at the symmetric positions with respect to the jet centerline (corresponding to the second and fourth quadrant in Fig. 5). It is considered that this negative correlation in the opposite sides of the jet centerline would be caused by the self-preserving zigzag array of counter-rotating vortices reported in many other researchers[10]-[14]. This feature is also understood as the appearance of the "jet flapping" phenomenon[10] which

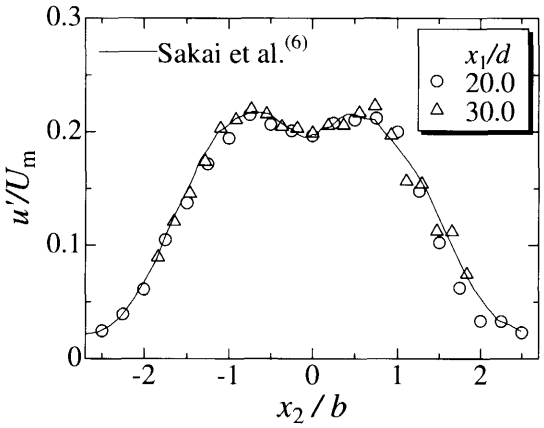

Fig. 4 Vertical profiles of the streamwise r.m.s. velocity u'

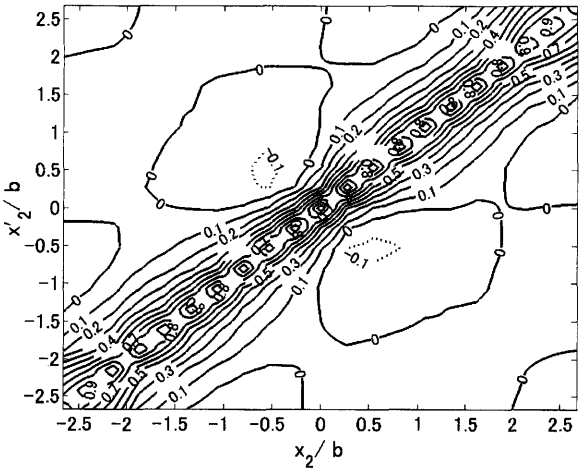

Fig. 5 Distribution of the spatial correlation coefficient C_{uu} at $x_1/d = 20.0$

was suggested as one of the large scale structures in the turbulent plane jet.

4.3 Time variation of the streamwise velocity field

The term "flapping" is named from the visual image of this phenomenon that the jet flaps as a flag does. However, in authors' knowledge, there are almost no studies by which the entity of the flapping phenomenon could be captured. And in general, the jet "flapping" itself is not well known in comparison with other coherent structures, for example, the bursting[1] phenomena in a turbulent boundary layer. So more detail examination on the dynamics of the "flapping" phenomenon is necessary. Figures 6 (a) and (b) show the time variation of the streamwise total velocity field $\tilde{u}(x_2,t) = U(x_2) + u(x_2,t)$ and the streamwise fluctuating velocity field $u(x_2,t)$ at $x_1/d = 20.0$. The abscissa is time [sec], the ordinate denotes x_2 normalized by the half width b, and the gradation scale shows the value of the streamwise velocity [m/s]. The time interval shown in Fig. 6 is a part of the whole sampling time (about 23 sec), in which the flapping seems to be occurring. From Fig. 6 (a), it is observed that the region with high velocity moves up and down as time proceeds, and it is thought that this result expresses the feature of the flapping as mentioned above. From Fig. 6 (b), it is found that fluid lumps with the positive and negative streamwise fluctuating velocity on opposite sides of the jet centerline exist almost alternately. This structure causes the negative value of C_{uu} of the jet centerline.

5. Results of the KL Expansion

5.1 Eigenvalues

Figure 7 presents the distributions of the eigenvalue $\lambda_u^{(n)}$ and the cumulative eigenvalues $\sum_{i=1}^{n}\lambda^{(i)}$ at $x_1/d = 20.0$. The abscissa gives the number of modes of the KL expansion n. $\lambda_u^{(n)}$ and $\sum_{i=1}^{n}\lambda^{(i)}$ are normalized by the integral of the mean square value of the fluctuating velocity u, i.e., the sum of all eigenvalues $\lambda_{\text{total}} = \sum_{i=1}^{21}\lambda^{(i)}$. Consequently the value of the ordinates means the (cumulative) contribution of each mode (first n modes) to the sum of all eigenvalues. The solid line and the broken line in Fig. 7 show the results of the simultaneous measurements at two points with the X-type hot-wire probes at $x_1/d = 20.0$[6], and it is found that they agree well with the present results by the multi-point simultaneous measurements. The energy contribution of the first mode and the second mode contains approximately 23% and 17%, respectively. The contribution for the sum of first three modes is about 50% and the sum of first seven modes captures nearly 80%.

5.2 Eigenfunctions

In the present experiments, the total number of eigenfunctions (modes) is $N = 21$, which corresponds to the number of probes. Here we devide these modes into three ranges, i.e., low-numbered modes ($n = 1 \sim 5$), middle-numbered modes ($n = 6 \sim 10$) and higher-numbered modes ($n = 11 \sim 21$), then the characteristics of modes in each range are investigated. Figures 8 (a) – (c) show profiles of the eigenfunctions $\phi_u^{(n)}(x_2)$ at $x_1/d = 20.0$, where (a) gives the profiles of the representatives of low-numbered modes ($n = 1, 2$), (b) the ones of middle-numbered modes ($n = 7, 9$) and (c) the ones of higher-numbered modes ($n = 14, 19$). It is ascertained that the present profiles agree with the ones of the simultaneous measurements at two points with the X-type probes at $x_1/d = 20.0$[6]. Here, we discuss the shapes of the eigenfunctions. Firstly, the low-numbered modes (in particular the first mode) in Fig. 8 (a) are considered. The profile of the first mode $\phi_u^{(1)}$ is the shape like a sine curve. This shape gives an effect of acceleration at one side of the jet and deceleration at another side. Therefore, $\phi_u^{(1)}$ plays the role of making the two-point streamwise correlation C_{uu} on opposite sides of the jet centerline negative. This is consistent with the "flapping"[10]–[14] which is a characteristic

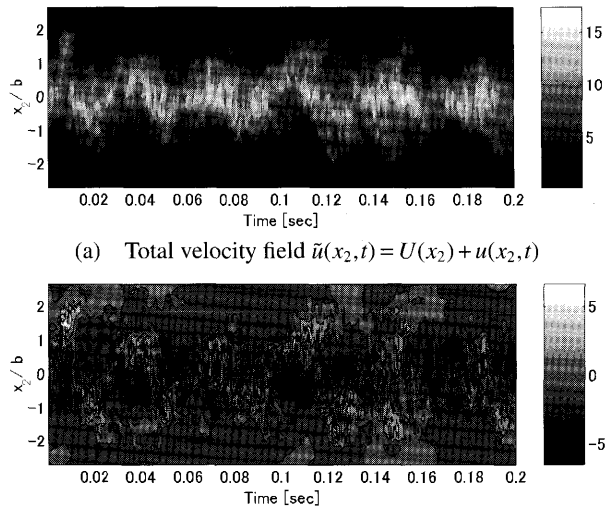

(a) Total velocity field $\tilde{u}(x_2,t) = U(x_2) + u(x_2,t)$

(b) Fluctuating velocity field $u(x_2,t)$

Fig. 6 Time variations of the spatial velocity field at $x_1/d = 20.0$

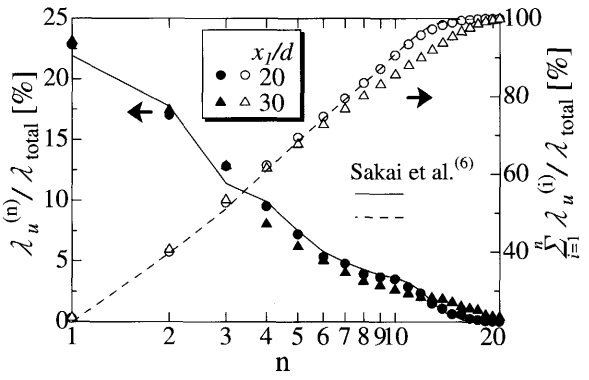

Fig. 7 Distribution of the eigenvalues at $x_1/d = 20.0$

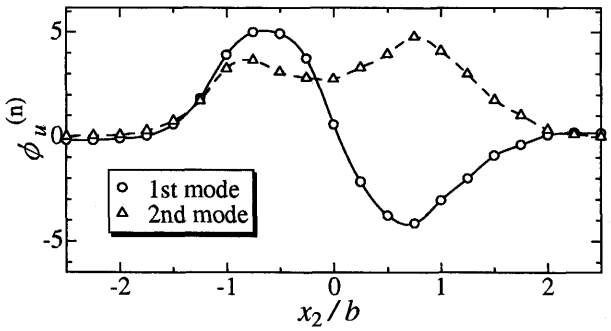

(a) Eigenfunctions of $n = 1$ and 2

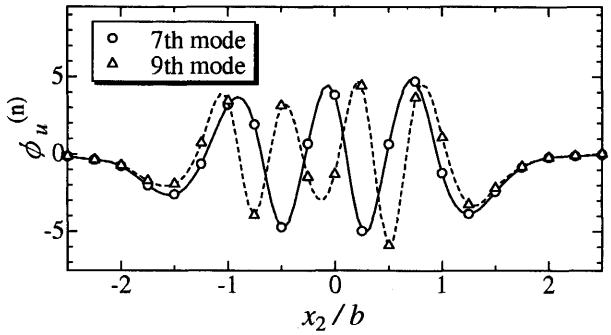

(b) Eigenfunctions of $n = 7$ and 9

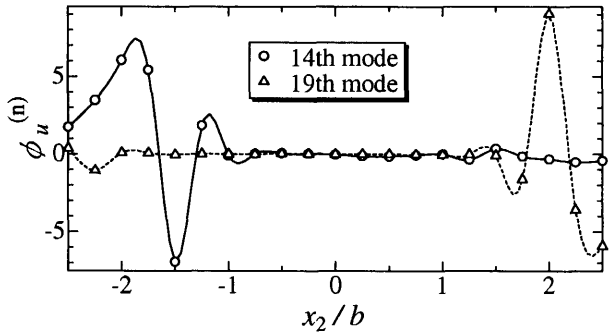

(c) Eigenfunctions of $n = 14$ and 19

Fig. 8 Profiles of the eigenfunctions at $x_1/d = 20.0$

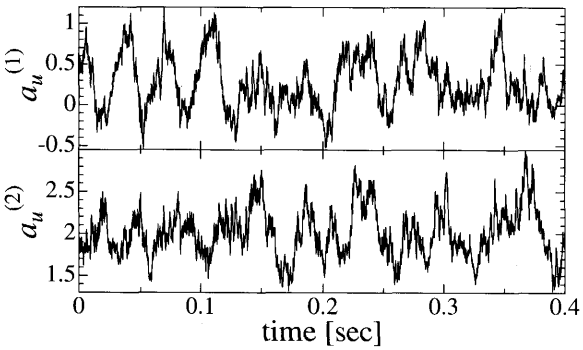

(a) Random coefficients of $n = 1$ and 2

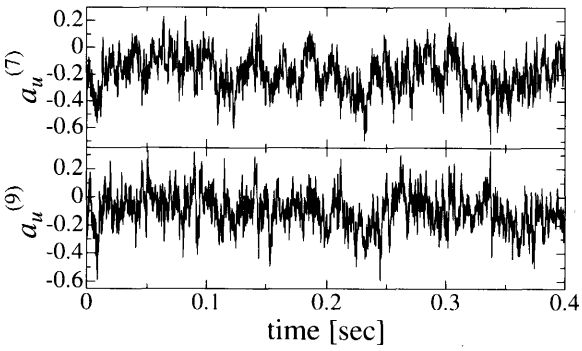

(b) Random coefficients of $n = 7$ and 9

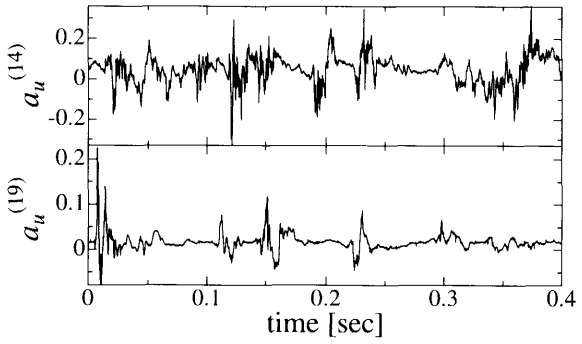

(c) Random coefficients of $n = 14$ and 19

Fig. 9 Time variations of the random coefficients at $x_1/d = 20.0$

structure in the self-preserving region. It is also understood that the feature of the negative C_{uu} on opposite sides of the jet centerline is due to the most energetic structure in the self-preserving region, i.e., the first mode of the KL expansion. Secondly, from the profiles of the 7th mode $\phi_u^{(7)}$ and the 9th mode $\phi_u^{(9)}$ in Fig. 8 (b), it is found that the middle-numbered modes represent finer (small-scale) structures because more peaks appear in comparison with low-numbered modes (see Fig. 8 (a)). Finally, the higher-numbered modes in Fig. 8 (c) are considered. It is found that the profile of the 14th mode $\phi_u^{(14)}$ and 19th mode $\phi_u^{(19)}$ shows almost zero near the jet centerline and a sharp peak in the outer edge. This means that the higher-numbered modes contribute mainly to the flow structure for the outer edge of the jet.

5.3 Random coefficients

Figures 9 (a) – (c) show the time variations of the random coefficients $a_u^{(n)}(t)$ at $x_1/d = 20.0$ which correspond to the eigenfunctions in Figs. 8 (a) – (c), i.e., Fig. 9 (a) is for the low-numbered modes (n = 1, 2), Fig. 9 (b) is for the middle-numbered modes (n = 7, 9) and Fig. 9 (c) is for the higher-numbered modes (n = 14, 19). The KL expansion enables to decompose a turbulent velocity field $u(x_2,t)$ to random coefficients $a_u^{(n)}(t)$ depending on only time and eigenfunctions $\phi_u^{(n)}(x_2)$ depending on only space. Therefore it can be generally considered that $a_u^{(n)}(t)$ has the random information and $\phi_u^{(n)}(x_2)$ has the deterministic one. From Fig. 9, it is found that these time variations of $a_u^{(n)}(t)$ have different properties depending on n. Firstly, it is observed that the coefficients of low-numbered modes (the 1st mode $a_u^{(1)}$ and the 2nd mode $a_u^{(2)}$) in Fig. 9 (a) include the small fluctuations, but the large fluctuation is dominant as a whole. Secondly, the coefficients of middle-numbered modes (the 7th mode $a_u^{(7)}$ and the 9th mode $a_u^{(9)}$) in Fig. 9 (b) are almost random signals. Finally, co-

efficients of higher-numbered modes (the 14th mode $a_u^{(14)}$ and the 19th mode $a_u^{(19)}$) in Fig. 9 (c) show the intermittent property. From the above features of the random coefficients and the profiles of their corresponding eigenfunctions (modes), it is suggested that the modes of the KL expansion are classified as follows: the low-numbered modes corresponding to the large scale (coherent) structure, the middle-numbered modes corresponding to the small scale random structure and the higher-numbered modes corresponding to the intermittent structure in the outer edge.

5.4 Reconstruction of the streamwise velocity field

Figures 10 (a) and (b) show the reconstructed fluctuating velocities at $x_1/d = 20.0$ using first n modes $u^{(n)}(x_2,t) = \sum_{i=1}^{n} a_u^{(i)}(t)\phi_u^{(i)}(x_2)$ (see Eq. (5)). In Fig. 10, the gray lines present original signals and the black lines present the reconstructed ones. Figure 10 (a) gives the signals at the central part of the jet ($x_2/b = 0.75$), and the cumulative contributions $\lambda_u^{(n)}/\lambda_{\text{total}}$ for 2, 5 and 10 are 39.7%, 68.5% and 90.9%, respectively. Figure 10 (b) presents the signals near the outer edge ($x_2/b = 2.24$), and the cumulative contributions for 5, 13 and 17 are 68.5%, 97.2% and 99.7%, respectively. Here, it should be noticed that the increase of the cumulative contribution (the increase of n) does not necessarily correspond to the efficiency of a signal reconstruction. This reason is described in the following. Firstly the signals at $x_2/b = 0.75$ are considered. From Fig. 10 (a), it is found that for the signal of $u^{(2)}$ large-scale fluctuations are reconstructed well, but the reconstruction of fine-scale fluctuations is poor. For the signal of $u^{(5)}$, large-scale fluctuations are almost the same shapes as the one of $u^{(2)}$, but the fine fluctuations are reconstructed more sufficiently. The reconstructed signal of $u^{(10)}$ becomes indistinguishable from the original one. Therefore Fig. 10 (a) shows the successful case that the cumulative contribution (the increase of n) corresponds very well to the reconstruction of a signal. The reason is that the eigenfunctions of lower-numbered modes have large magnitudes at the central part of the jet (see Figs. 8 (a) and (b)) so that the reconstruction can be made efficiently by only low-numbered modes. On the other hand, in Fig. 10 (b), it is found that the reconstruction of a signal hardly proceeds in using lower-numbered modes and needs higher-numbered modes. Therefore the cumulative contribution (the increase of n) does not correspond well to the reconstruction of a signal near the outer edge. The reason is that lower-numbered modes have small magnitudes at the outer edge (see Figs. 8 (a) and (b)) and mainly higher-numbered modes (see Fig. 8 (c)) contribute to the reconstruction of a signal at this position.

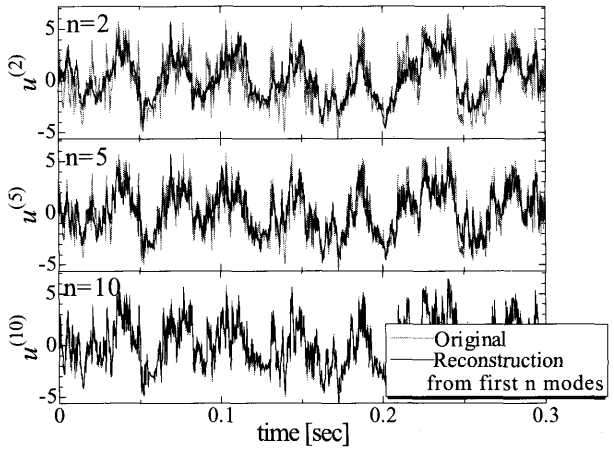

(a) At the central part of the jet ($x_2/b = 0.75$)

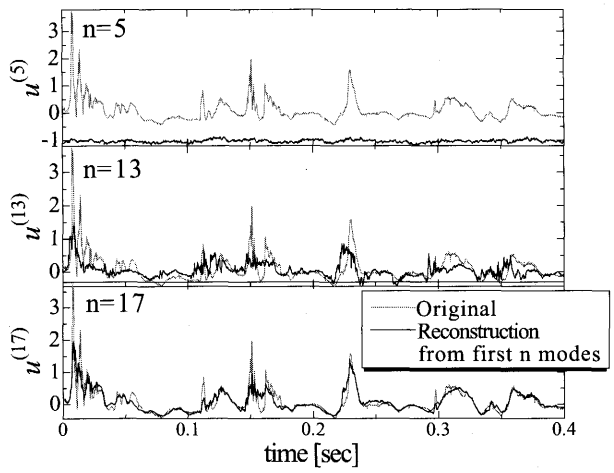

(b) Near the outer edge ($x_2/b = 2.24$)

Fig. 10 Reconstruction of the fluctuating velocity at $x_1/d = 20.0$

5.5 Time variation of the spatial distribution of reconstructed velocity field

Figures 11 (a) – (c) show the time variations of the fluctuation velocity field reconstructed from first n modes, i.e., $u^{(n)}(x_2,t) = \sum_{i=1}^{n} a^{(i)}(t)\phi_u^{(i)}(x_2)$ ((a): from the first mode ($n = 1$); (b): from first 2 modes ($n = 2$); (c): from first 10 modes ($n = 10$)). It is noticed that the time interval shown in Figs. 6 and 11 are same, and the reconstruction for $n = 21$ corresponds to Fig. 6 (b) (original field). From Fig. 11 (a), it is found that there exist pairs of fluid lumps with the positive ($u > 0$) and negative ($u < 0$) streamwise velocity fluctuation on the opposite sides of the jet centerline, and the signs of velocity fluctuation for fluid lumps changes alternately as time proceeds. In Fig. 11 (b), we also find the similar structure to Fig. 11 (a), but it is noticed that fluid lumps with the same signs pass through both sides of the jet centerline after about 0.13 sec. This is explained as follows. Since the first mode $\phi_u^{(1)}$ is point-symmetric with respect to $x_2/b = 0.0$ (see Fig. 8 (a)), the sign of u reverses at $x_2/b > 0$ and $x_2/b < 0$, whereas the second mode $\phi_u^{(2)}$ which gives the same effect on the velocity field for both sides of the jet (see Fig. 8 (a)). In the present case, it can be understood that the effect of

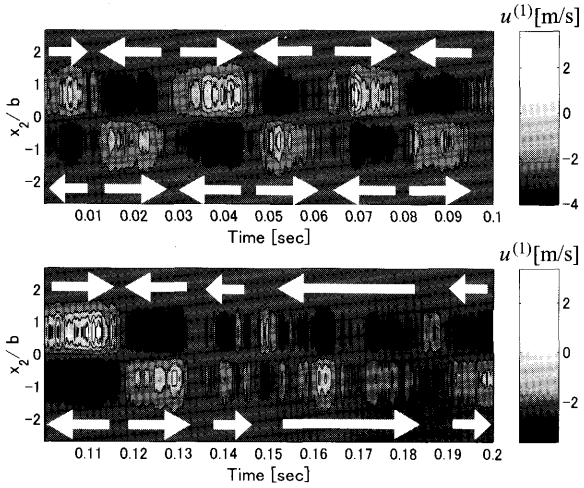

(a) Reconstructed velocity from the first mode

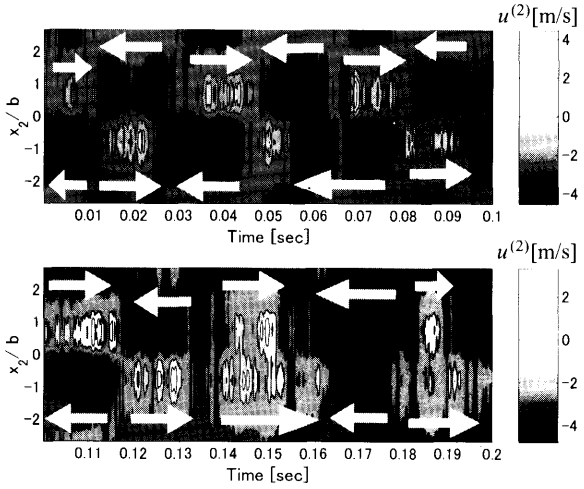

(b) Reconstructed velocity from first 2 modes

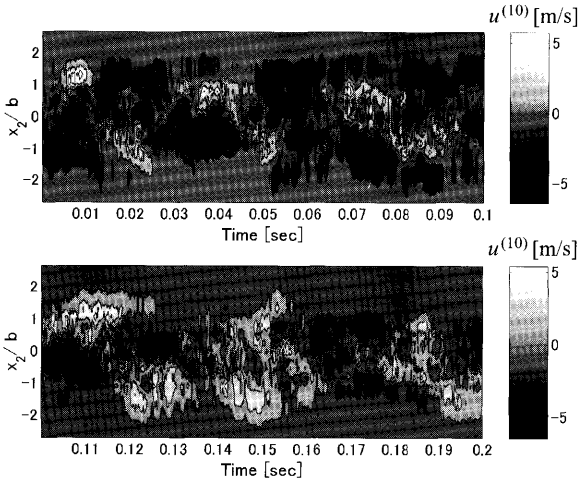

(c) Reconstructed velocity from first 10 modes

Fig. 11 Time variations of the spatial distribution of reconstructed velocity field at $x_1/d = 20.0$

$\phi_u^{(2)}$ becomes more effective to the fluctuating velocity after 0.13 sec. (note: the mean energy contributions of $\phi_u^{(1)}$ and $\phi_u^{(2)}$ to the total energy are not so different, i.e., $\phi_u^{(1)}$: 23%, $\phi_u^{(2)}$: 17%, as shown in Fig. 7). Furthermore

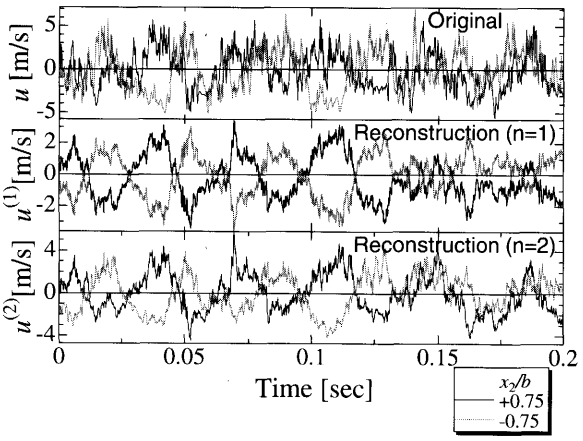

Fig. 12 Reconstructed fluctuating velocity on opposite sides of the jet centerline at $x_1/d = 20.0$

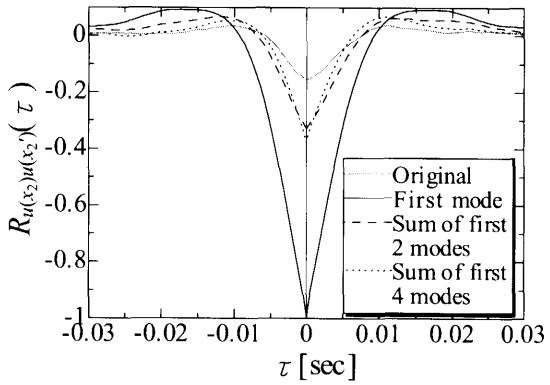

Fig. 13 Profiles of the two-point spatial velocity coefficient for the original velocity signal and the reconstructed velocity signals at $x_2/b = \pm 0.75$, $x_1/d = 20.0$

from Figs. 11 (b) and (c), it is found that fine and complex structures are reconstructed more clearly as the number of mode (n) increases.

Figure 12 shows time variations of the original fluctuating velocity $u(x_2,t)$ and the reconstructed fluctuating velocity $u^{(n)}(x_2,t)$ at $x_2/b = \pm 0.75$. The upper figure shows original signals, and the middle and lower figures are signals reconstructed from the first mode and first 2 modes, respectively. From Fig. 12, it is found that reconstructed signals at $x_2/b = \pm 0.75$ present the inverse motion to each other (strong negative correlation). Further, these reconstructed signals (in particular $n = 1$ and $n = 2$) show shapes like a sine curve, and this feature means that large scale vortices pass periodically (see Figs. 11 (a) and (b)). Figure 13 shows the two-point spatial velocity correlation coefficient $R_{u(x_2)u(x_2')} = \left\langle u^{(n)}(x_2,t)u^{(n)}(x_2',t)\right\rangle$ for the original velocity $u(x_2,t)$ and the reconstructed velocity $u^{(n)}(x_2,t)$, which are measured at the same positions as Fig. 12 (at $x_2/b = \pm 0.75$). From the figure, it is found that the profile for the original velocity signal shows the value -0.15 at $\tau = 0$, and the one for the reconstructed velocity signal from the first mode shows a very strong negative value

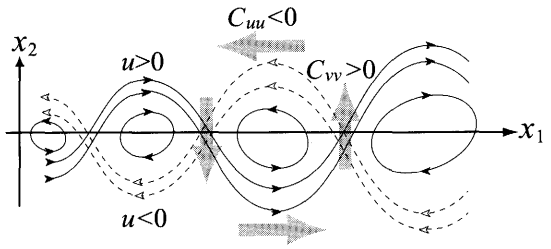

Fig. 14 The first mode model of jet's flapping phenomenon by the KL expansion

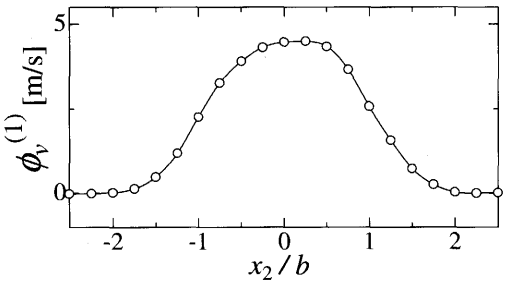

Fig. 15 Profile of the first eigenfunction of v, $\phi_v^{(1)}$ from Sakai et al.[6]

-1.0 at $\tau = 0$. Further, the ones for the reconstructed velocity signals from first 2 and 4 modes show -0.33 which is two times as large as the one for the original velocity signal.

Now, we suggest the simple model of the jet flapping phenomenon shown in Fig. 14. This model is constructed on the basis of the profiles of the first mode of u, i.e., $\phi_u^{(1)}$ (see Fig. 8 (a)), the first mode of v, i.e., $\phi_v^{(1)}$ (see Fig. 15[6], v: the cross-streamwise fluctuating velocity) and the reconstructed velocity field $u^{(1)}(x_2,t)$ in the time interval that the flapping is occuring (see Fig. 11 (a)). The flow structure shown in Fig. 14 is explained as follows. Figure 8 (a) shows that the profile of $\phi_u^{(1)}$ takes a shape like sine curve with zero crossing at $x_2/b = 0$ and the maximum (minimum) value at $x_2/b \approx \pm 0.75$. In contrast, from Fig. 15, it is found that the profile of $\phi_v^{(1)}$ shows a symmetric shape with respect to the jet centerline ($x_2/b = 0$), and this shape has the same effect on the velocity field for both sides of the jet (i.e., if the flow is accelerated (decelerated) at one side of the jet flow field, then the flow at another side is also accelerated (decelerated)), so the two-point spatial velocity correlation of v, C_{vv}, becomes positive for opposite sides of the jet centerline[6]. Consequently, we can suppose the vortex structure whose center locates in the jet centerline by combination of $\phi_u^{(1)}$ and $\phi_v^{(1)}$. From Fig. 11 (a), it is also found that the sign of the vorticity changes alternately as time proceeds. For these reasons, it is considered that the flapping phenomenon is caused by the array of counter-rotating vortices whose center locates in the jet centerline like Fig. 14. Here, it should be noticed that the model of the organized structures in the self-preserving region of a plane jet are also suggested

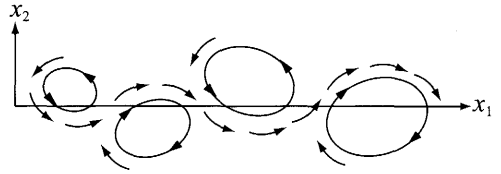

Fig. 16 Schematic of coherent structure in a plane jet from Antonia et al.[12]

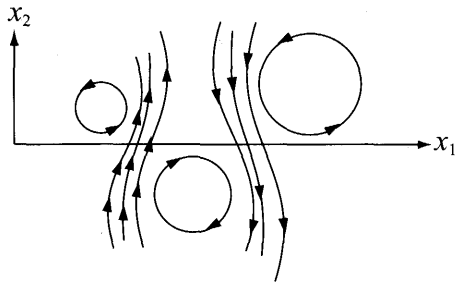

Fig. 17 Schematic of coherent structure in a plane jet from Thomas and Brehob[14]

by Antonia et al.[12] and Thomas and Brehob[14]. These models are shown in Figs. 16 and 17 for comparison with the present model. They suggested the zigzag array of counter-rotating vortices with respect to the jet centerline. However, the present model in Fig. 14 does not show the zigzag array. This is because the present model is suggested on the basis of only the first mode of the KL expansion, by which the state of the real structure of a plane jet in the self-preserving region may be not expressed precisely. If the modes of higher number than $n = 1$ are considered, it seems that the zigzag structure can be obtained like other researchers.

Finally, we will give the brief comment on the probability that the flapping occurs. We devided the whole sampling time into a lot of short-time intervals of which each length is taken to be the inverse of the flapping frequency[10]-[12] at $x_2/b = \pm 0.75$. Then we calculated the two-point velocity correlation coefficient. The result was that the probability of showing the strong negative correlation smaller than about -0.3 is about 17% in the whole sampling time. This probability agrees more or less with the energy contribution rate of the first mode. However, this probability is for the one-cycle flapping, so it is considered that the probability for several cycles of the flapping to occur as observed in Fig. 6 is very low. This is a reason that makes it difficult to capture visually the jet flapping phenomenon.

6. Conclusions

The simultaneous measurements of the main streamwise velocity at 21 points in the self-preserving region of a turbulent plane jet have been performed by an array of I-type hot-wire probes. Then the KL expansion was applied to investigate the coherent structure.

(1) From the results of the mean velocity, the r.m.s. velocity, the two-point spatial velocity correlation, and the eigenvalues and the eigenfunctions of the KL expansion, the reliability of the present multi-point measurement system is confirmed.

(2) From the relationship between the random coefficients and the eigenfunctions, it is found that the low-numbered, middle-numbered and higher-numbered modes represent the large-scale (coherent) structure, the finer (small-scale) random structure and the intermittent structure in the outer edge, respectively.

(3) From the velocity field reconstructed by the first KL mode, it is found that there exist a pair of fluid lumps with the positive and negative streamwise velocity fluctuation on the opposite sides of the jet centerline, and the signs of velocity fluctuation for fluid lumps changes alternately as time proceeds. These characteristics are consistent with the "jet flapping" phenomenon.

References

(1) Blackwelder, R.F. and Kaplan, R.E., On the Wall Structure of the Turbulent Boundary Layer, J. Fluid. Mech., Vol.76, No.1 (1976), pp.89–112.

(2) Holmes, P., Lumley, J.L. and Berkooz, G., Turbulence, Coherent Structures, Dynamical Systems and Symmetry, (1996), pp.86–128, Cambridge Univ. Press.

(3) Lumley, J.L., The Structure of Inhomogeneous Turbulent Flows, Atmospheric Turbulence and Radio Wave Propagation, Edited by Yaglom, A.M. and Tatarsky, V.I., (1967), pp.166–178, Nauka, Moscow.

(4) Gordeyev, S.V. and Thomas, F.O., Coherent Structure in the Turbulent Planar Jet. Part 1. Extraction of Proper Orthogonal Decomposition Eigenmodes and Their Self-Similarity, J. Fluid Mech., Vol.414 (2000), pp.145–194.

(5) Gordeyev, S.V. and Thomas, F.O., Coherent Structure in the Turbulent Planar Jet. Part 2. Structural Topology via POD Eigenmode Projection, J. Fluid Mech., Vol.460 (2002), pp.349–380.

(6) Sakai, Y., Tanaka, N. and Kushida, T., On the Development of Coherent Structure in a Plane Jet (Part 1, Characteristics of Two-Point Velocity Correlation and Analysis of Eigenmodes by the KL Expansion), JSME Int. J., Ser.B, Vol.49, No.1 (2006), pp.115–124.

(7) Sakai, Y., Tanaka, N. and Kushida, T., On the Development of Coherent Structure in a Plane Jet (Part 2, Investigation of Spatio-Temporal Velocity Structure by the KL Expansion), JSME Int. J., Ser.B, Vol.49, No.3 (2006), pp.714–721.

(8) Tanaka, N., Sakai, Y., Kushida, T. and Kuribara, T., A Study on the Realization of a Turbulent Plane Jet with the High Two-Dimensionality by Means of Both the Skimmer and the Side Wall, and Investigation of Its Fundamental Property, Fluid & Heat Engineering Research, (in Japanese), Vol.39, No.1 (2004), pp.9–16.

(9) Hino, M., Spectrum Analysis, (in Japanese), (1977), pp.52–55, Asakura Press.

(10) Goldschmidt, V.W. and Bradshow, P., Flapping of a Plane Jet, Phys. Fluids, Vol.16, No.3 (1973), pp.354–355.

(11) Cervantes de Gortari, J. and Goldschmidt, V.W., The Apparent Flapping Motion of a Turbulent Plane Jet—Further Experimental Results, J. Fluid Eng., Vol.103 (1981), pp.119–126.

(12) Antonia R.A., Chambers, A.J., Britz, D. and Browne, L.W.B., Organized Structures in a Turbulent Plane Jet, J. Fluid. Mech., Vol.134 (1983), pp.49–66.

(13) Oler, J.W. and Goldschmidt, V.W., A Vortex-Street Model of the Flow in the Similarity Region of a Two-Dimensional Free Turbulent Plane Jet, J. Fluid. Mech., Vol.123 (1982), pp.523–535.

(14) Thomas, F.O. and Brehob, E.G., An Investigation of Large Scale Structure in the Similarity Region of a Two-Dimensional Turbulent Jet, Phys. Fluids, Vol.29, No.6 (1973), pp.1788–1795.